ISSN 1674-1056
http://cpb.iphy.ac.cn
http://iopscience.iop.org/cpb
中国物理 B
Chinese Physics
中国物理 Chinese Physics B

Efficient doping modulation of monolayer WS_2 for optoelectronic applications

Xinli Ma(马新莉), Rongjie Zhang(张荣杰), Chunhua An(安春华), Sen Wu(吴森), Xiaodong Hu(胡晓东), Jing Liu(刘晶)

Citation: Chin. Phys. B . 2019, 28(3): 037803. **doi:** 10.1088/1674-1056/28/3/037803
Journal homepage: http://cpb.iphy.ac.cn; http://iopscience.iop.org/cpb

What follows is a list of articles you may be interested in

Influences on oxidation voltage and holding time on poly(3-methylthiophene) film for electrochromic stability

Bo Zhang(张波), Chen Xu(徐晨), Guo-Yue Xu(徐国跃), Chu-Yang Liu(刘初阳), Hong-Han Bu(卜红寒), Jian-Chao Zhang(张建超)

Chin. Phys. B . 2018, 27(12): 127802. **doi:** 10.1088/1674-1056/27/12/127802

Spin-current pump in silicene

John Tombe Jada Marcellino, Mei-Juan Wang(王美娟), Sa-Ke Wang(汪萨克), Jun Wang(汪军)

Chin. Phys. B . 2018, 27(5): 057801. **doi:** 10.1088/1674-1056/27/5/057801

Optimizing effective phase modulation in coupled double quantum well Mach-Zehnder modulators

Guang-Hui Wang(王光辉), Jin-Ke Zhang(张金珂)

Chin. Phys. B . 2018, 27(2): 027801. **doi:** 10.1088/1674-1056/27/2/027801

Different angle-resolved polarization configurations of Raman spectroscopy: A case on the basal and edge plane of two-dimensional materials

Xue-Lu Liu(刘雪璐), Xin Zhang(张昕), Miao-Ling Lin(林妙玲), Ping-Heng Tan(谭平恒)

Chin. Phys. B . 2017, 26(6): 067802. **doi:** 10.1088/1674-1056/26/6/067802

Tunable band gap and optical properties of surface functionalized Sc_2C monolayer

Shun Wang(王顺), Yu-Lei Du(杜宇雷), Wen-He Liao(廖文和)

Chin. Phys. B . 2017, 26(1): 017806. **doi:** 10.1088/1674-1056/26/1/017806

SPECIAL TOPIC — Photodetector: Materials, physics, and applications

Efficient doping modulation of monolayer WS_2 for optoelectronic applications*

Xinli Ma(马新莉), Rongjie Zhang(张荣杰), Chunhua An(安春华), Sen Wu(吴森), Xiaodong Hu(胡晓东), and Jing Liu (刘晶)†

State Key Laboratory of Precision Measurement Technology and Instruments, School of Precision Instruments and Opto-electronics Engineering, Tianjin University, Tianjin 300072, China,

(Received 28 November 2018; revised manuscript received 27 December 2018; published online 23 January 2019)

Transition metal dichalcogenides (TMDCs) belong to a subgroup of two-dimensional (2D) materials which usually possess thickness-dependent band structures and semiconducting properties. Therefore, for TMDCs to be widely used in electronic and optoelectronic applications, two critical issues need to be addressed, which are thickness-controllable fabrication and doping modulation of TMDCs. In this work, we successfully obtained monolayer WS_2 and achieved its efficient doping by chemical vapor deposition and chemical doping, respectively. The n- and p-type dopings of the monolayer WS_2 were achieved by drop coating electron donor and acceptor solutions of triphenylphosphine (PPh_3) and gold chloride ($AuCl_3$), respectively, on the surface, which donates and captures electrons to/from the WS_2 surface through charge transfer, respectively. Both doping effects were investigated in terms of the electrical properties of the fabricated field effect transistors. After chemical doping, the calculated mobility and density of electrons/holes are around 74.6/39.5 $cm^2 \cdot V^{-1} \cdot s^{-1}$ and $1.0 \times 10^{12}/4.2 \times 10^{11}$ cm^{-2}, respectively. Moreover, we fabricated a lateral WS_2 p–n homojunction consisting of non-doped n-type and p-doped p-type regions, which showed great potential for photodetection with a response time of 1.5 s and responsivity of 5.8 A/W at $V_G = 0$ V and $V_D = 1$ V under 532 nm light illumination.

Keywords: two-dimensional materials, tungsten disulfide, chemical doping, homojunction, photodetector

PACS: 78.20.Jq, 42.79.Hp, 42.70.Gi **DOI:** 10.1088/1674-1056/28/3/037803

1. Introduction

Recently, two-dimensional (2D) transition metal dichalcogenides (TMDCs) have attracted increasing interest due to their unique physical, chemical, and mechanical properties.[1–6] In addition, most TMDCs possess thickness-dependent band structures,[7–9] which transition from indirect to direct bandgap as the thickness is thinned from multi- to mono-layer, such as monolayer molybdenum disulfide (MoS_2), tungsten disulfide (WS_2), selenide molybdenum ($MoSe_2$), etc.[10] The direct bandgaps of monolayer TMDCs are ideal for electronic and optoelectronic applications.[11,12] Current means of fabricating monolayer TMDCs mainly involve two methods: mechanical exfoliation of monolayer TMDCs from the bulk counterpart and chemical vapor deposition (CVD) of monolayer TMDCs. As compared to mechanical exfoliation, CVD is a promising way to produce large-area monolayer TMDCs with high quality, which can potentially implement wafer-scale device fabrication.[13–15] Further doping the CVD grown monolayer TMDCs is another important aspect to fabricating functional devices, which is usually achieved by applying gate voltage, laser excitation, chemical doping, etc. Among these methods, chemical doping is considered an effective method to modulate the carrier type and concentration of the material.[16–18]

In this work, we successfully grew monolayer WS_2 by the CVD method and efficiently modulated both n- and p-type dopings of WS_2 by drop chemical doping. The WS_2 is one type of TMDC known for its high photoluminescence (PL) quantum yield and high electron mobility predicted by theoretical calculation. The capability of growing large-area monolayer WS_2 makes it a promising candidate for semiconducting optoelectronics and micro/nanoelectronics.[19–21] The chemical doping-enabled n- and p-type modulations are through drop coating triphenylphosphine (PPh_3) and gold chloride ($AuCl_3$) on the surface of WS_2, which are a typical electron dopant and acceptor, respectively, to cause electron transfer between the coating layer and the WS_2 surface.[22,23] The method of surface coating has effectively enhanced both the electron/hole mobility and density of WS_2 to 74.6/39.5 $cm^2 \cdot V^{-1} \cdot s^{-1}$ and $1.0 \times 10^{12}/4.2 \times 10^{11}$ cm^{-2}, respectively. This result suggests the feasibility of making a p–n homojunction on a single WS_2 flake, which is favorable for photodetection, since the built-in potential can significantly lower the dark current and power consumption.[24] Herein, we fabricated a WS_2 p–n homojunction on a single WS_2 flake which consisted of a non-doped n-type region and an $AuCl_3$ coated p-type region. This fabricated device showed an effective photoresponse to visible light. The method is expected to promote the application and development of monolayer WS_2

*Project supported by the National Natural Science Foundation of China (Grant No. 21405109) and Seed Foundation of State Key Laboratory of Precision Measurement Technology and Instruments, China (Grant No. 1710).

†Corresponding author. E-mail: jingliu_1112@tju.edu.cn

© 2019 Chinese Physical Society and IOP Publishing Ltd

toward tunnel diodes, light-emitting diodes (LEDs), photodetectors, and solar cells.

2. Experimental details

2.1. CVD growth process of WS_2

Monolayer WS_2 crystals were grown on the ⟨100⟩ oxidized silicon substrates (SiO_2 (285 nm)/Si (500 μm)) under atmospheric pressure condition. The set-up of the furnace is shown in Fig. 1(a). The growth process was conducted in a quartz tube furnace with two heating zones. WO_3 (10 mg, 99.9% purity, Aladdin) and S (500 mg, 99.9% purity, Aladdin) powders were chosen as the precursor materials.[25,26] Before growth, 2 cm × 2 cm SiO_2 substrate was cleaned by ultrasonicating in acetone, isopropanol, and deionized water sequentially for 10 min, respectively. After the substrate was dried in nitrogen flow, it was placed face-down above the ceramic boat containing WO_3 in the second heating zone. The ceramic boat containing S was placed around 20 cm away from WO_3 in the first heating zone.

First of all, a flow of high-purity (99.999%) Ar at 500 sccm was introduced to remove the residual oxygen in the tube for about 1 h. After that, the Ar flow was decreased to 200 sccm during the growth as the carrier gas. The temperature variation curves of the growth are shown in Fig. 1(b). The temperature of WO_3 was first quickly raised from room temperature to 800 °C with a heating rate of 10 °C /min and then slowly raised to 900 °C with a heating rate of 5 °C/min. At the same time, the temperature of the sulfur powder reached 180 °C with a heating rate of 10 °C /min. Then, the temperatures of sulfur powder and WO_3 powder were kept at 900 °C and 180 °C, respectively. The holding time was around 10 min to make sure that the monolayer WS_2 was formed and deposited on the substrate. Finally, the growth process ended after cooling the system from elevated to room temperature naturally.

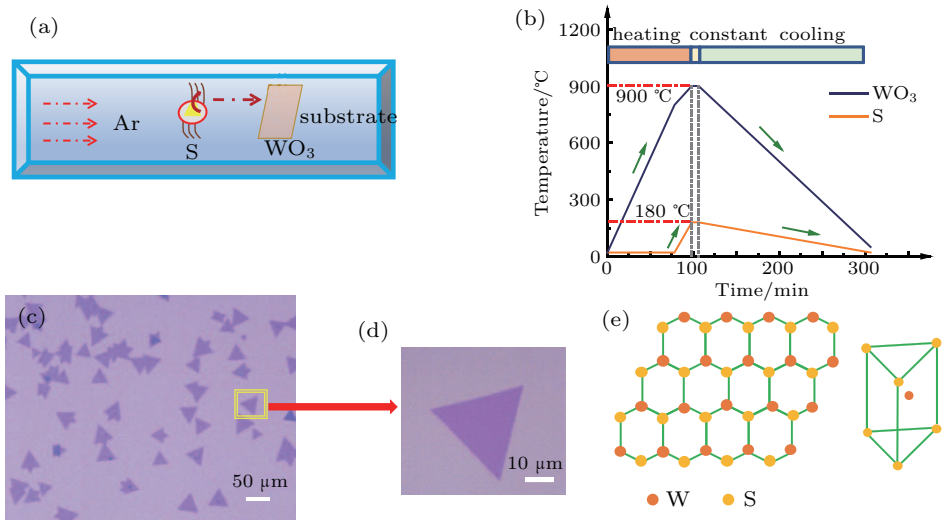


Fig. 1. Growth of monolayer WS_2. (a) Experimental set-up of the CVD furnace. (b) Temperature variation curves of WO_3 and S during CVD growth. (c), (d) Optical images of the as-grown WS_2. (e) Molecular structure of the monolayer WS_2.

2.2. Characterization of monolayer WS_2

The thickness and surface morphology of monolayer WS_2 transferred on SiO_2/Si substrate were characterized by atomic force microscope (AFM, Bruker, Germany). Raman spectroscopy and photoluminescence (PL) analysis were performed using a Renishaw InVia Raman microscope with an excitation laser wavelength of 532 nm, laser power of 10 mW, and laser spot size of ∼ 1 μm. The scan ranges were from 300 cm^{-1} to 550 cm^{-1} for Raman analysis and from 580 cm^{-1} to 700 nm for PL measurement. All the tests were conducted at room temperature in ambient atmosphere.

2.3. Transfer and fabrication of WS_2 FET devices

In order to fabricate the WS_2 field effect transistor (FET), the CVD-grown WS_2 flake was transferred from the growth substrate to the patterned SiO_2/Si substrate. The transfer process is shown in Fig. 2. Firstly, the SiO_2/Si substrate with CVD-grown WS_2 flakes was spin-coated by polymethyl methacrylate (PMMA) 950 at 2000 r.p.m. for 60 s. Secondly, the PMMA-coated sample was baked at 150 °C for 10 min, after which the edges of the sample were cut. Thirdly, the sample was soaked in 10% KOH at 80 °C for about 2 h, during which the PMMA/WS_2 film was exfoliated from the SiO_2/Si substrate and floated on the surface of the liquid. Then, the patterned SiO_2/Si substrate was used to refloat the PMMA/WS_2 films followed by deionized water rinsing several times. After that, the sample was baked at 150 °C for 10 min again to reinforce the adhesion between the film and substrate. Finally, the PMMA was washed with acetone and isopropanol, leaving monolayer WS_2 transferred on the patterned SiO_2/Si substrate. After electron beam lithography, the metal electrodes of Ti (10 nm)/Au (30 nm) were deposited on the transferred WS_2 flake by electron beam evaporating and sequential lifting-off processes.[27]

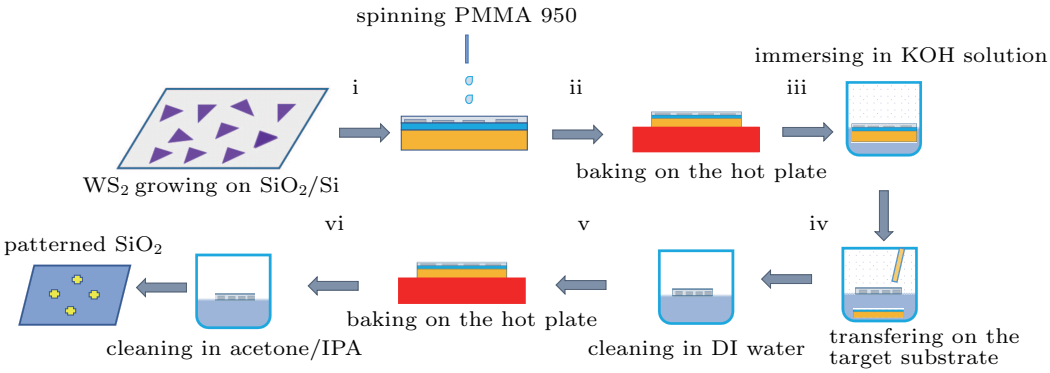


Fig. 2. Wetting transfer process of the WS_2 grown SiO_2/Si substrate.

2.4. Doping and characterization of the devices

The chemical doping solution was prepared by dissolving 5 mmol $PPh_3/AuCl_3$ in 1 mL methylbenzene/nitromethane to serve as the n/p-dopant. For doping, a drop of solution was coated on the WS_2 flake and dried at 50 °C. The p–n homojunction was fabricated by drop coating p-dopant solutions on half of the WS_2 flake using hexagonal boron nitride (h-BN) as the cover mask.[28]

The electrical properties (transfer and output characteristics) of the FET devices were measured using a B1500 semiconductor analyzer (Agilent, USA). Photoelectrical responses of the device were measured by AOTF-Pro laser and B1500 semiconductor analyzer.

The carrier mobility was calculated by the equation[16,29]

$$u = [\mathrm{d}I_\mathrm{D}/\mathrm{d}V_\mathrm{G}] \times [L/(W \cdot V_\mathrm{D} \cdot C_\mathrm{i})],$$

where $\mathrm{d}I_\mathrm{D}/\mathrm{d}V_\mathrm{G}$ is the transconductance, and L, W, and C_i represent the channel length, the channel width, and the capacitance between the channel and the back gate, respectively. The carrier density was calculated by the equation[23]

$$n = (I_\mathrm{D} \cdot L)/(q \cdot W \cdot V_\mathrm{D} \cdot u),$$

where q is the electron charge, I_D is the source–drain current at zero gate voltage, V_D is the source–drain voltage, and μ is the field-effect carrier mobility.

3. Results and discussion

3.1. Characterization of monolayer WS_2

The optical images of the WS_2 flakes grown on the SiO_2/Si substrate are shown in Fig. 1(c), which present typical triangle shapes. It is consistent with the sandwiched molecular structure and triangular symmetry of monolayer WS_2 as shown in Fig. 1(e). The lateral dimension of the crystal is larger than 40 μm. Besides, the single WS_2 flake presented in Fig. 1(d) is approximately an equilateral triangle, suggesting that the flake is a single crystal without extended defects or grain boundaries.[12,30] Figure 3(a) shows the AFM image of a WS_2 flake on SiO_2/Si substrate, which exhibits a smooth surface and homogeneous thickness except for the central part. Generally, the CVD-grown WS_2 exhibits a pyramidal-type structure, in which the central part usually consists of several atomic layers while the boundary area only has one atomic layer.[31,32] Therefore, the thickness profile measured by AFM, Raman and photoluminescence (PL) spectra were all obtained from the boundary area. In the AFM measurement, the cross-sectional height of the WS_2 flake in Fig. 3(b) is ~ 0.74 nm, which corresponds to a monolayer WS_2 as previously reported.[20,33] Figures 3(c) and 3(d) show the Raman and PL spectra of the WS_2 flake, respectively. In Fig. 3(c), two obvious peaks of WS_2 are observed in the Raman spectrum within the range from 300 cm^{-1} to 550 cm^{-1}. One peak located near 355 cm^{-1} represents the in-plane phonon modes of E^1_{2g}, while the other peak at 415 cm^{-1} represents the out-of-plane phonon modes of A_{1g}. Such a Raman spectrum is consistent with previously reported ones. The separation between the two characteristic peaks is around 59 cm^{-1}, which is

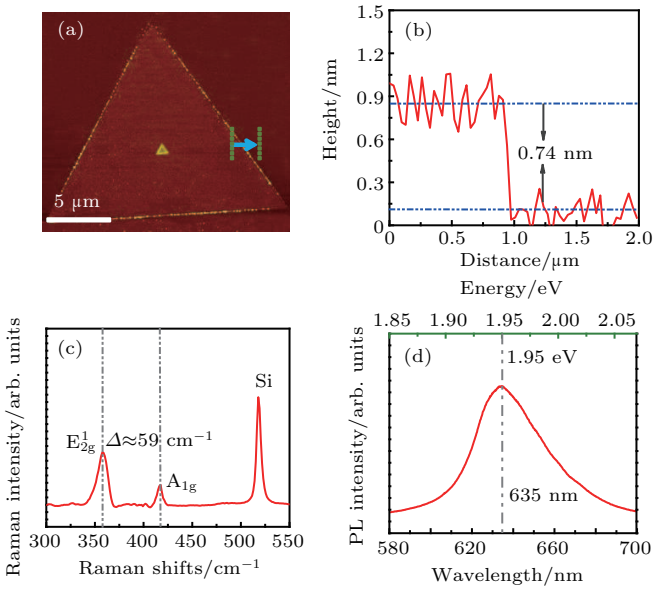


Fig. 3. Characterization of CVD-grown WS_2. (a) AFM image, (b) thickness profile, (c) Raman and (d) photoluminescence spectra of the CVD-grown monolayer WS_2.

equal to the reported values of monolayer WS_2.[34] Besides, the PL spectrum in Fig. 3(d) shows a single sharp peak located near 1.95 eV (corresponds to 635 nm), which is in accordance with the bandgap of monolayer WS_2.[20]

3.2. Electrical properties of the monolayer WS_2 FET

To evaluate the electrical characteristics, we transferred monolayer WS_2 onto SiO_2/Si substrate and fabricated it into an FET, the optical topography of which is shown in Fig. 4(a). Figures 4(b)–4(d) present the transfer curves in linear and logarithmic scale and the output characteristics of the device, respectively. According to Figs. 4(b) and 4(c), the non-doped material is a typical n-type semiconductor with calculated field-effect carrier mobility of 14.1 $cm^2 \cdot V^{-1} \cdot s^{-1}$. The on-state current is 2.2 μA with an achieved on/off current ratio of up to 10^6 within ±60 V gate bias. In the output curves, the drain current increases with the source–drain and gate bias. The nonlinear characteristic of the drain current versus source–drain bias indicates a Schottky barrier existing at the Ti/Au metal contact.

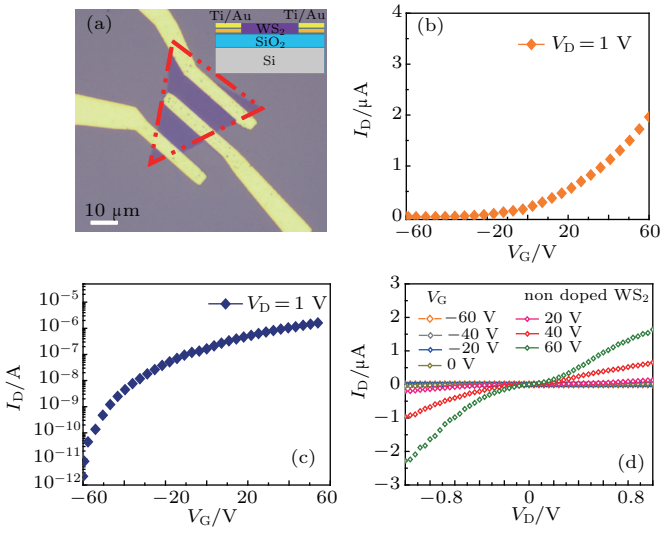


Fig. 4. Electrical properties of the monolayer WS_2 FET. (a) Optical topography of the device. (b), (c) Transfer characteristic curves of the device in (b) linear and (c) logarithmic scale. (d) Output characteristics of the device.

3.3. Electrical properties of the n- and p-doped WS_2 FETs

Figure 5 shows the modulation of the chemical doping on the electrical properties of WS_2 FET. Figure 5(a) illustrates the chemical doping mechanism by PPh_3 and $AuCl_3$. When coated with the PPh_3 layer, the electrons transferred from PPh_3 to WS_2, resulting in n-type doping in WS_2.[22] Figures 5(b) and 5(c) are the representative transport characteristics of a WS_2 FET before and after drop coating 5 mmol/ml PPh_3, respectively, in which the threshold voltage of the WS_2 FET shifts to a more negative value, indicating the n-doping effect. In addition, the on-state current increases from 2.2 μA to 12.3 μA and the on/off current ratio decreases to 10 within ±60 V gate bias after n-doping. The output curves of n-doped WS_2 also become more linear and symmetric than those of the pristine one, as shown in Fig. 5(d), owing to the improved Ohmic contact between n-doped WS_2 and the Ti electrodes. Based on these transport characteristics, we further calculated the electron mobility and density after n-doping, which achieved 74.6 $cm^2 \cdot V^{-1} \cdot s^{-1}$ and 1.0×10^{12} cm^{-2}, respectively. The calculated electron density is comparable to the values achieved by other chemical doping solutions to monolayer WS_2, such as pentamethylrhodocene dimer (in the concentration of 2.1×10^{12} cm^{-2}) and 2, 3, 5, 6 tetrafluoro-7, 7, 8, 8-tetracyanoquinodimethane (in the concentration of 6.0×10^{12} cm^{-2}).[35,36]

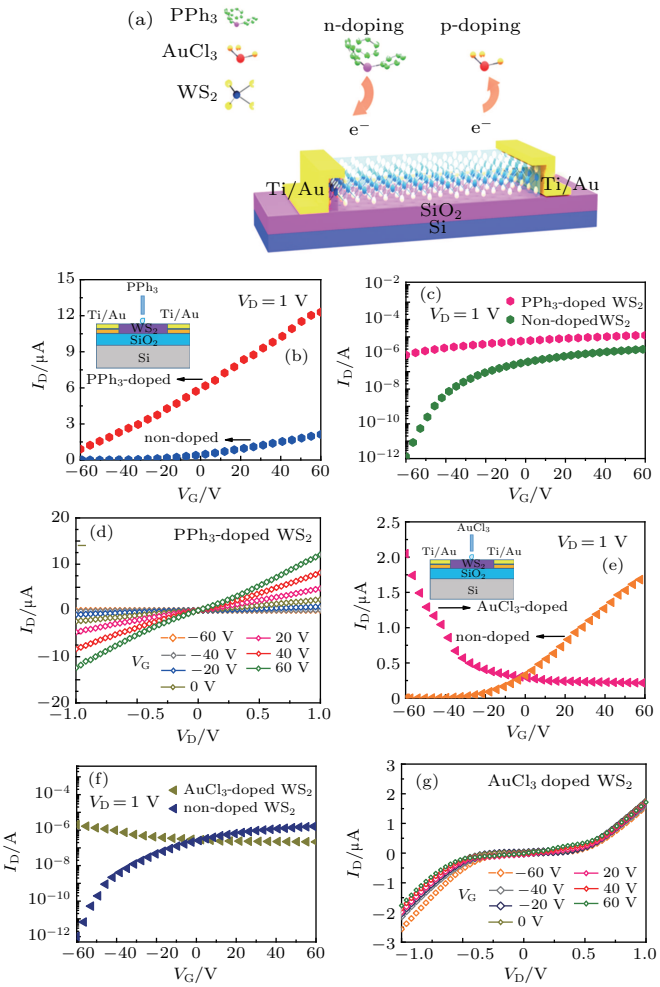


Fig. 5. Electrical properties of the chemically doped WS_2 FETs. (a) Schematic illustration of the chemical doping mechanism. (b), (c) Transfer characteristic curves of WS_2 FET in (b) linear and (c) logarithmic scale before and after PPh_3 coating. (d) Output characteristics of PPh_3-doped WS_2 FET. (e), (f) Transfer characteristic curves of WS_2 FET in (e) linear and (f) logarithmic scale before and after $AuCl_3$ coating. (g) Output characteristics of $AuCl_3$-doped WS_2 FET.

On the other hand, the Au^{3+} ions can be reduced and thus electrons are extracted from WS_2 to induce the p-doping effect.[23] The transfer curves of the WS_2 FET before and after p-doping treatment by 5 mmol/ml $AuCl_3$ are shown in Figs. 5(e) and 5(f), respectively, which transferred from n-

to p-type after $AuCl_3$ coating. The on-state current shows a variation from 1.8 μA to 2.1 μA with on/off current ratio decreased to 10 within ±60 V gate bias after p-doping. The calculated hole mobility and density are 39.5 $cm^2 \cdot V^{-1} \cdot s^{-1}$ and 4.2×10^{11} cm^{-2}, respectively. Such a doping level is comparable or even better than the values achieved by introducing nitrogen atoms into WS_2.[37,38] Figure 5(g) shows the output curves of the device after p-type doping under various gate bias, which become less linear than the pristine device, indicating a higher Schottky barrier due to an increased difference between the work functions of Ti and $AuCl_3$-doped monolayer WS_2.

3.4. Electrical and photoelectrical properties of the lateral WS_2 p–n homojunction

In Fig. 6, we demonstrate a lateral WS_2 p–n homojunction with enhanced optoelectronic performance as compared to a pristine WS_2 FET. Figure 6(a) shows the structure diagram of the device. The n-type area of WS_2 was the pristine WS_2 covered by a BN flake, while the p-type area was fabricated by drop coating 5 mmol/mL $AuCl_3$ on the surface of the WS_2 device. Figure 6(b) shows the output curves of the WS_2 p–n homojunction under various gate bias voltages ranging from −40 V to 40 V. Figure 6(c) presents one representative output curve of the diode under a forward bias of 1 V and 0 V gate bias in the logarithmic scale. The ideality factor of the device is calculated to be 1.35 by the equation $I = I_S(e^{V_D/nVT} - 1)$,[39] where I is the diode current, I_S is the reverse bias saturation current, V_D is the voltage across the diode, n is the ideality factor, and V_T is the thermal voltage. It implies a very low charge-trap density at the homojunction interface of the diode. Figure 6(d) exhibits the optical response of the p–n homojunction diode under 532 nm light illumination at the gate bias of $V_G = 0$ V and the source–drain bias of $V_D = 1$ V. The WS_2 p–n homojunction presents the response and recovery for the light illumination within 1.5 s on average. We calculated the photoresponsivity of the p–n homojunction to be 5.8 A/W at $V_G = 0$ V and $V_D = 1$ V by the equation photoresponsivity $= I_{ph}/P_{light}$,[40,41] where I_{ph} is the generated photocurrent and P_{light} represents the total incident optical power on the device. The photoresponsivity of this device is comparable to that of the lateral p–n homojunctions made by $MoSe_2$, WSe_2, and MoS_2, which are 1.3 A/W, 3 A/W, and 5.07 A/W, respectively.[24,28,42]

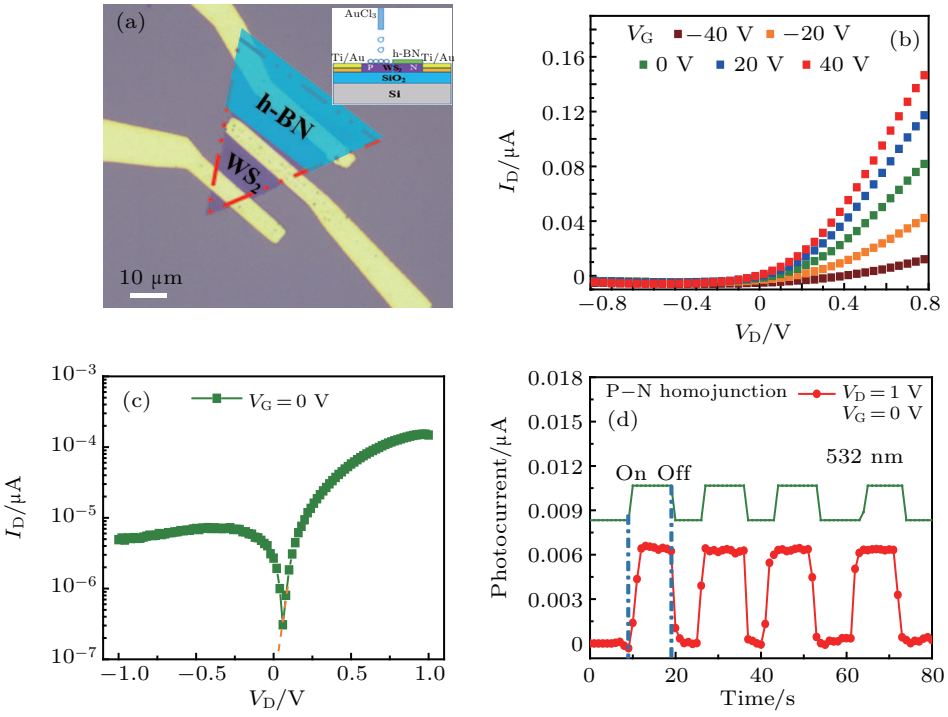


Fig. 6. Electrical and photoelectrical properties of the WS_2 lateral p–n homojunction. (a) Structure diagram of the device. Inset is the schematic of the device. (b), (c) Output characteristic curves of the device in (b) linear and (c) logarithmic scale at $V_G = 0$ V. (d) Dynamic photoresponse of the device.

4. Conclusion

In summary, we successfully obtained monolayer WS_2 flakes by the CVD method, which were characterized by AFM, Raman and PL spectra. By drop coating PPh_3 and $AuCl_3$ solutions on the surface of the monolayer WS_2, we can effectively n- and p-dope the WS_2, and thus modulate the electrical properties of the WS_2 FET, including on-state current, on/off ratio, and carrier mobilities. Finally, we realized a p–n homojunction on a single WS_2 flake, which consisted of pristine and $AuCl_3$ p-doped areas in one WS_2 flake. The p–n diode achieved a photoresponsivity of 5.8 A/W to 532 nm

light illumination under $V_G = 0$ V and $V_D = 1$ V with a response/recovery time of 1.5 s.

References

[1] Tedstone A A, Lewis D J and O'Brien P 2016 *Chem. Mater.* **28** 1965
[2] Mak K F, He K, Shan J and Heinz T F 2012 *Nat. Nanotechnol.* **7** 494
[3] Zhan Y, Liu Z, Najmaei S, Ajayan P M and Lou J 2012 *Small* **8** 966
[4] Gu P, Zhang K, Feng Y, Wang F, Miao Y, Han Y and Zhang H 2016 *Acta Phys. Sin.* **65** 018102 (in Chinese)
[5] Wang W, Kang Z, Song Q, Wang X, Deng J, Ding X and Che J 2018 *Acta Phys. Sin.* **67** 240601
[6] Zeng F, Zhang W and Tang B 2015 *Chin. Phys. B* **24** 097103
[7] Tongay S, Fan W, Kang J, Park J, Koldemir U, Suh J, Narang D S, Liu K, Ji J, Li J, Sinclair R and Wu J 2014 *Nano Lett.* **14** 3185
[8] Wei X, Yan F, Shen C, Lv Q and Wang K 2017 *Chin. Phys. B* **26** 038504
[9] Zhang X and Li Q 2016 *Chin. Phys. B* **25** 117103
[10] Liu Y, Weiss N O, Duan X, Cheng H C, Huang Y and Duan X 2016 *Nat. Rev. Mater.* **1** 16042
[11] Zeng H, Dai J, Yao W, Xiao D and Cui X 2012 *Nat. Nanotechnol.* **7** 490
[12] Gao Y, Liu Z, Sun D M, Huang L, Ma L P, Yin L C, Ma T, Zhang Z, Ma X L, Peng L M, Cheng H M and Ren W 2015 *Nat. Commun.* **6** 8569
[13] Manzeli S, Ovchinnikov D, Pasquier D, Yazyev O V and Kis A 2017 *Nat. Rev. Mater.* **2** 17033
[14] Li X and Zhu H W 2015 *J. Materiomics* **1** 33
[15] Shi Y, Li H and Li L J 2015 *Chem. Soc. Rev.* **44** 2744
[16] Sim D M, Kim M, Yim S, Choi M J, Choi J, Yoo S and Jung Y S 2015 *ACS Nano.* **9** 12115
[17] Kang D H, Kim M S, Shim J, Jeon J, Park H Y, Jung W S, Yu H Y, Pang C H, L S and Park J H 2015 *Adv. Funct. Mater.* **25** 4219
[18] Li Z, Hu Y, Li Y and Fang Z 2017 *Chin. Phys. B* **26** 036802
[19] Georgiou T, Yang H, Jalil R, Chapman J, Novoselov K S and Mishchenko A 2014 *Dalt. Trans.* **43** 10388
[20] Yue Y, Chen J C, Zhang Y, Ding S S, Zhao F, Wang Y, Zhang D, Li R J, Dong H, Hu W, Feng Y and Feng W 2018 *ACS. Appl. Mater. Interfaces.* **10** 22435
[21] Cong C, Shang J, Wang Y and Yu T 2018 *Adv. Opt. Mater.* **6** 1700767
[22] Jo S H, Kang D H, Shim J, Jeon J, Jeon M H, Yoo G, Kim J, Lee J, Yeom G Y, Lee S, Yu H Y, Choi C and Park J H 2016 *Adv. Mater.* **28** 4824
[23] Liu X, Qu D, Ryu J, Ahmed F, Yang Z, Lee D and Yoo W J 2016 *Adv. Mater.* **28** 2345
[24] Choi M S, Qu D, Lee D, Liu X, Watanabe K, Taniguchi T and Yoo W J 2014 *ACS Nano.* **8** 9332
[25] Zhang Q, Lu J, Wang Z, Dai Z, Zhang Y, Huang F, Bao Q, Duan W, Fuhrer M S and Zheng C 2018 *Adv. Opt. Mater.* **6** 1701347
[26] Lan C, Li C, Yin Y and Liu Y 2015 *Nanoscale* **7** 5974
[27] Wang A X, Kang K, Chen S and Du R 2017 *2D. Mater.* **4** 025093
[28] Fan S, Shen W, An C, Sun Z, Wu S, Xu L, Sun D, Hu X, Zhang D and Liu J 2018 *ACS Appl. Mater. Interfaces.* **10** 26533
[29] Zhang R, Xie Z, An C, Fan S, Zhang Q, Wu S, Xu L, Hu X, Zhang D, Sun D, Chen J and Liu J 2018 *ACS Appl. Mater. Interfaces.* **10** 27840
[30] Kim M S, Yun S J, Lee Y, Seo C, Han G H, Kim K K, Lee Y H and Kim J 2016 *ACS Nano.* **10** 2399
[31] Thangaraja A, Shinde S M, Kalita Golap and Tanemura M 2015 *Mater. Lett.* **156** 156
[32] Cong C, Shang J, Wu X, Cao B, Peimyoo N, Qiu C, Sun L and Yu T 2014 *Adv. Opt. Mater.* **2** 131
[33] Feng S, Yang R, Jia Z, Xiang J, Wen F, Nie C M A, Zhao Z, Xu B, Tao C, Tian Y and Liu Z 2017 *ACS Appl. Mater. Interfaces.* **9** 34071
[34] Yang W, Shang J, Wang J, Shen X, Cao B, Peimyoo N, Zou C, Chen Y, Wang Y, Cong C, Huang W and Yu T 2016 *Nano Lett.* **16** 1560
[35] Zhang S, Hill H M, Moudgil K, Richter C A, Hight Walker A R, Barlow S, Marder S R, Hacker C A and Pookpanratana S J 2018 *Adv. Mater.* **30** 1802991
[36] Peimyoo N, Yang W, Shang J, Shen X, Wang Y and Yu T 2014 *ACS Nano.* **8** 11320
[37] Tang B, Yu Z G, Huang L, Chai J, Wong S L, Deng J, Yang W, Gong H, Wang S, Ang K and Zhang Y 2018 *ACS Nano.* **12** 2506
[38] Cao Q, Dai Y, Xu J, Chen L, Zhu H, Sun Q and Zhang D W 2017 *ACS Appl. Mater. Interfaces.* **9** 18215
[39] Xin W, Li X, He X, Su B, Jiang X, Huang K, Zhou X, Liu Z and Tian J 2018 *Adv. Mater.* **30** 1704653
[40] Yin Z, Li H, Li H, Jiang L, Shi Y M, Sun Y H, Lu G, Zhang Q, Chen X D and Zhang H 2012 *ACS Nano.* **6** 74
[41] Zhang Z, Kang Z, Liao Q, Zhang X and Zhang Y 2017 *Chin. Phys. B.* **26** 118102
[42] Zhou C, Zhao Y, Raju S, Wang Y, Lin Z, Chan M and Chai Y 2016 *Adv. Mater.* **26** 4223